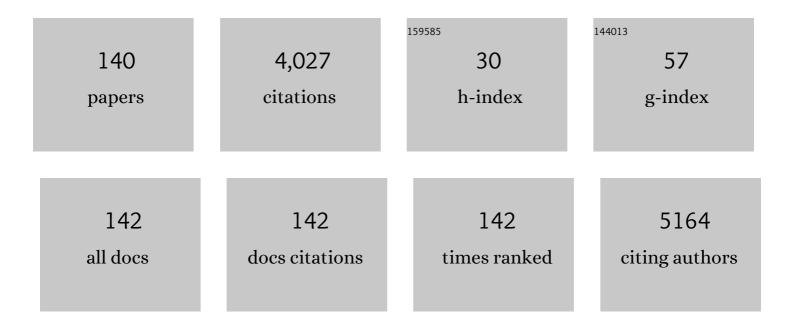
## Long Zhang

List of Publications by Year in descending order

Source: https://exaly.com/author-pdf/1426958/publications.pdf Version: 2024-02-01



#	Article	IF	CITATIONS
1	Time-resolved online analysis of the gas- and particulate-phase of cigarette smoke generated by a heated tobacco product using vacuum ultraviolet photoionization mass spectrometry. Talanta, 2022, 238, 123062.	5.5	4
2	Ultrafast Optical Properties of Cavityâ€Enhanced Superfluorescence. Advanced Optical Materials, 2022, 10, .	7.3	8
3	Low thermal expansion ZBLANâ€based glass ceramics containing CaZrF <sub>6</sub> crystals. Journal of the American Ceramic Society, 2022, 105, 3959-3966.	3.8	2
4	Switchable ultra-broadband terahertz wave absorption with VO2-based metasurface. Scientific Reports, 2022, 12, 2501.	3.3	30
5	Next generation mid-infrared fiber: fluoroindate glass fiber. Optical Materials Express, 2022, 12, 1683.	3.0	18
6	Relaxation Oscillations of an Exciton–Polariton Condensate Driven by Parametric Scattering. Nano Letters, 2022, 22, 3026-3032.	9.1	7
7	Er3+ concentration-dependent microstructural and upconversion luminescence process of transparent perfluoride composite glass. Journal of the European Ceramic Society, 2022, 42, 4335-4342.	5.7	7
8	Luminescence and structural evolution in ultraâ€low melting quaternary tin fluorophosphate glasses (NaFâ€SnF <sub>2</sub> â€SnOâ€P <sub>2</sub> O <sub>5</sub> ). Journal of the American Ceramic Society, 2022, 105, 2595-2604.	3.8	2
9	Nanolayered VO <sub>2</sub> -Based Switchable Terahertz Metasurfaces as Near-Perfect Absorbers and Antireflection Coatings. ACS Applied Nano Materials, 2022, 5, 5569-5577.	5.0	17
10	Enhanced near-infrared transmission of ZnO-doped Y2O3–MgO nanocomposites with reduced light scattering due to decreased refractive index difference. Journal of the European Ceramic Society, 2022, 42, 4616-4622.	5.7	5
11	A novel approach and segregation behavior of heavily doped Nd:YAG/YAG composite structure by solid-state crystal growth. Optical Materials, 2022, 128, 112455.	3.6	0
12	Solventâ€Mediated Structural Evolution in Colloidal Lead Halide Perovskite Nanocrystals Selfâ€Assembly. Advanced Materials Interfaces, 2022, 9, .	3.7	1
13	Solventâ€Mediated Structural Evolution in Colloidal Lead Halide Perovskite Nanocrystals Selfâ€Assembly (Adv. Mater. Interfaces 19/2022). Advanced Materials Interfaces, 2022, 9, .	3.7	0
14	On fast LuAG:Ce scintillation ceramics with Ca <sup>2+</sup> coâ€dopants. Journal of the American Ceramic Society, 2021, 104, 966-973.	3.8	8
15	Tunable and transparent broadband metamaterial absorber with water-based substrate for optical window applications. Nanoscale, 2021, 13, 7831-7837.	5.6	44
16	Ultrastable low-cost colloidal quantum dot microlasers of operative temperature up to 450 K. Light: Science and Applications, 2021, 10, 60.	16.6	25
17	Defects & Luminescence of Lu <sub>3</sub> Al <sub>5</sub> O <sub>12</sub> Phosphor Doped with Na Ion. Chemistry Letters, 2021, 50, 1359-1362.	1.3	1
18	Joint latent low-rank and non-negative induced sparse representation for face recognition. Applied Intelligence, 2021, 51, 8349.	5.3	8

#	Article	IF	CITATIONS
19	Transparent ultra-wideband double-resonance-layer metamaterial absorber designed by a semiempirical optimization method. Optics Express, 2021, 29, 18446.	3.4	17
20	Fabrication of infrared-transparent Y2O3–MgO composites using nanopowders synthesized via thermal decomposition. Ceramics International, 2021, 47, 13007-13014.	4.8	7
21	Broadening emission band of Yb:LuScO 3 transparent ceramics for ultrashort pulse laser. Journal of the American Ceramic Society, 2021, 104, 6064-6073.	3.8	3
22	Preparation and study of the mechanical and optical properties of infrared transparent Y <sub>2</sub> O <sub>3</sub> –MgO composite ceramics. Journal of the American Ceramic Society, 2021, 104, 6335-6344.	3.8	7
23	Quantum Dot Selfâ€Assembly Enables Lowâ€Threshold Lasing. Advanced Science, 2021, 8, e2101125.	11.2	28
24	Demonstration of Thermally Tunable Multi-Band and Ultra-Broadband Metamaterial Absorbers Maintaining High Efficiency during Tuning Process. Materials, 2021, 14, 5708.	2.9	8
25	Femtosecond-scale all-optical switching in oxyfluorogallate glass induced by nonlinear multiphoton absorption. RSC Advances, 2021, 11, 32446-32453.	3.6	8
26	Samarium and manganese incorporation to improve color rendering of LuAG:Ce <sup>3+</sup> phosphor ceramics for laser-driven lighting: a Color-tunable and energy transfer study. Journal of Materials Chemistry C, 2021, 9, 16468-16476.	5.5	6
27	Phase-Type Fresnel Zone Plate with Multi-Wavelength Imaging Embedded in Fluoroaluminate Glass Fabricated via Ultraviolet Femtosecond Laser Lithography. Micromachines, 2021, 12, 1362.	2.9	5
28	CHEMICAL MECHANICAL POLISHING AND ITS MECHANISM ON YTTERBIUM-DOPED MIXED SESQUIOXIDES (Yb:LuScO <sub>3</sub> ). Surface Review and Letters, 2021, 28, 2050036.	1.1	0
29	Surface Structure and Electronic Properties of Lu3Al5O12. Crystals, 2021, 11, 1433.	2.2	6
30	Linearly polarized lasing based on coupled perovskite microspheres. Nanoscale, 2020, 12, 5805-5811.	5.6	22
31	Heatâ€driven Tailored for Eliminating Nd 3+ Reâ€clusters in Nd 3+ ,Gd 3+ â€codoped SrF 2 Laser Ceramic. Journal of the American Ceramic Society, 2020, 103, 2562-2568.	3.8	7
32	Broad-band lead halide perovskite quantum dot single-mode lasers. Journal of Materials Chemistry C, 2020, 8, 13642-13647.	5.5	24
33	Er <sup>3+</sup> â€doped CaF <sub>2</sub> polycrystalline ceramic with perfect transparency for midâ€infrared laser. Journal of the American Ceramic Society, 2020, 103, 5808-5812.	3.8	5
34	Phase-separation engineering in fluorozirconate glass for designing and fabricating of transparent perfluorinate glass ceramic. Journal of the European Ceramic Society, 2020, 40, 3244-3248.	5.7	10
35	Near-field imaging of the multi-resonant mode induced broadband tunable metamaterial absorber. RSC Advances, 2020, 10, 5146-5151.	3.6	11
36	Allâ€Photonic Miniature Perovskite Encoder with a Terahertz Bandwidth. Laser and Photonics Reviews, 2020, 14, 1900398.	8.7	10

#	Article	IF	CITATIONS
37	Polariton–Polariton Interactions Revealed in a One-dimensional Whispering Gallery Microcavity. Nano Letters, 2020, 20, 1552-1560.	9.1	12
38	Energy transfer and wavelength tunable lasing of single perovskite alloy nanowire. Nano Energy, 2020, 71, 104641.	16.0	29
39	Cooperative excitonic quantum ensemble in perovskite-assembly superlattice microcavities. Nature Communications, 2020, 11, 329.	12.8	51
40	Large-scale, low-cost, broadband and tunable perfect optical absorber based on phase-change material. Nanoscale, 2020, 12, 5374-5379.	5.6	92
41	High-performance broadband electromagnetic interference shielding optical window based on a metamaterial absorber. Optics Express, 2020, 28, 26836.	3.4	41
42	Auger-type process in ultrathin ReS <sub>2</sub> . Optical Materials Express, 2020, 10, 1092.	3.0	17
43	Optical and thermal properties of TiO <sub>2</sub> â€doped Y <sub>2</sub> O <sub>3</sub> transparent ceramics synthesized by hot isostatic pressing. Journal of the American Ceramic Society, 2019, 102, 2021-2028.	3.8	14
44	Nonlinear Optical Signatures of the Transition from Semiconductor to Semimetal in PtSe <sub>2</sub> . Laser and Photonics Reviews, 2019, 13, 1900052.	8.7	64
45	Double-layer metal mesh etched by femtosecond laser for high-performance electromagnetic interference shielding window. RSC Advances, 2019, 9, 22282-22287.	3.6	28
46	An Allâ€Inorganic Perovskiteâ€Phase Rubidium Lead Bromide Nanolaser. Angewandte Chemie, 2019, 131, 16280-16286.	2.0	6
47	Surface-State Assisted Carrier Recombination and Optical Nonlinearities in Bulk to 2D Nonlayered PtS. ACS Nano, 2019, 13, 13390-13402.	14.6	37
48	An Allâ€Inorganic Perovskiteâ€Phase Rubidium Lead Bromide Nanolaser. Angewandte Chemie - International Edition, 2019, 58, 16134-16140.	13.8	12
49	Bacterially synthesized tellurium nanostructures for broadband ultrafast nonlinear optical applications. Nature Communications, 2019, 10, 3985.	12.8	68
50	Glass-forming ability control of Er3+-Doped lithium-modified fluorozirconate glass. Ceramics International, 2019, 45, 24115-24120.	4.8	4
51	High-Temperature Upconverted Single-Mode Lasing in 3D Fully Inorganic Perovskite Microcubic Cavity. ACS Photonics, 2019, 6, 793-801.	6.6	35
52	Femtosecond laser-induced damage characteristics of mid-infrared oxyfluorogallate glass. Optics and Laser Technology, 2019, 109, 659-665.	4.6	12
53	Highly-oriented (104) polycrystalline α-Al2O3 transparent ceramics prepared by a templated grain growth method. Journal of the European Ceramic Society, 2019, 39, 1721-1724.	5.7	9
54	Non-linear changes of performances caused by introduction of chloride ions into Er3+-doped fluorozirconate glass. Ceramics International, 2019, 45, 4431-4436.	4.8	4

#	Article	IF	CITATIONS
55	Fabrication of fine-grained undoped Y2O3 transparent ceramic using nitrate pyrogenation synthesized nanopowders. Ceramics International, 2019, 45, 5339-5345.	4.8	23
56	Perfluoride glass ceramic transmitting from UV to far-IR tailored by one step. Optics Letters, 2019, 44, 4857.	3.3	6
57	Facile synthesis and optical properties of colloidal quantum dots/ZnO composite optical resonators. RSC Advances, 2018, 8, 1778-1783.	3.6	3
58	Investigation of optical, mechanical, and thermal properties of ZrO2-doped Y2O3 transparent ceramics fabricated by HIP. Ceramics International, 2018, 44, 1362-1369.	4.8	29
59	YAG/Nd:LuAG composite laser materials prepared by the ceramization of YAG single crystals. Journal of the European Ceramic Society, 2018, 38, 1966-1971.	5.7	10
60	Effects of deformation rate on properties of Nd,Y-codoped CaF 2 transparent ceramics. Journal of the European Ceramic Society, 2018, 38, 2404-2409.	5.7	22
61	Single-mode lasing and 3D confinement from perovskite micro-cubic cavity. Journal of Materials Chemistry C, 2018, 6, 11740-11748.	5.5	37
62	Hybridization-induced broadband terahertz wave absorption with graphene metasurfaces. Optics Express, 2018, 26, 11728.	3.4	188
63	Ultrahigh Quality Upconverted Singleâ€Mode Lasing in Cesium Lead Bromide Spherical Microcavity. Advanced Optical Materials, 2018, 6, 1800391.	7.3	47
64	Facet-dependent nonlinear optical properties of bismuth oxychloride single-crystal nanosheets. Journal of Materials Chemistry C, 2018, 6, 8709-8716.	5.5	20
65	Structural Studies of NaPO <sub>3</sub> –AlF <sub>3</sub> Glasses by High-Resolution Double-Resonance Nuclear Magnetic Resonance Spectroscopy. Journal of Physical Chemistry C, 2018, 122, 21579-21588.	3.1	29
66	Grayscale image recording on Ge2Sb2Te5 thin films through laser-induced structural evolution. Scientific Reports, 2017, 7, 42712.	3.3	25
67	Fabrication of transparent yttria ceramics by alcoholic slip-casting. Ceramics International, 2017, 43, 8839-8844.	4.8	29
68	High transparency Cr,Nd:LuAG ceramics prepared with MgO additive. Journal of the European Ceramic Society, 2017, 37, 2459-2463.	5.7	10
69	Structural Studies of Bi <sub>2</sub> 0 <sub>3</sub> –NaPO <sub>3</sub> Glasses by Solid State Nuclear Magnetic Resonance and X-ray Photoelectron Spectroscopy. Journal of Physical Chemistry C, 2017, 121, 10087-10094.	3.1	3
70	Influence of synthesis conditions on the properties of Y2O3–MgO nanopowders and sintered nanocomposites. Journal of the European Ceramic Society, 2017, 37, 4095-4101.	5.7	15
71	Generic synthesis and versatile applications of molecularly organic–inorganic hybrid mesoporous organosilica nanoparticles with asymmetric Janus topologies and structures. Nano Research, 2017, 10, 3790-3810.	10.4	19
72	Perfectly transparent pore-free Nd3+-doped Sr9GdF21 polycrystalline ceramics elaborated from single-crystal ceramization. Journal of the European Ceramic Society, 2017, 37, 4912-4918.	5.7	13

#	Article	IF	CITATIONS
73	MoS <sub>2</sub> /Carbon Nanotube Core–Shell Nanocomposites for Enhanced Nonlinear Optical Performance. Chemistry - A European Journal, 2017, 23, 3321-3327.	3.3	57
74	Structural Studies of Fluoroborate Laser Glasses by Solid State NMR and EPR Spectroscopies. Journal of Physical Chemistry C, 2017, 121, 741-752.	3.1	21
75	Temperature dependent thermal conductivity and transition mechanism in amorphous and crystalline Sb2Te3 thin films. Scientific Reports, 2017, 7, 13747.	3.3	10
76	Influence of dopant concentration on the transparent and thermal properties of Nd 2 O 3 -doped alumina translucent ceramics. Journal of Rare Earths, 2017, 35, 883-886.	4.8	6
77	Single-Mode Lasers Based on Cesium Lead Halide Perovskite Submicron Spheres. ACS Nano, 2017, 11, 10681-10688.	14.6	216
78	Low-temperature-flux syntheses of ultraviolet-transparent borophosphates Na <sub>4</sub> MB <sub>2</sub> P <sub>3</sub> O <sub>13</sub> (M = Rb, Cs) exhibiting a second-harmonic generation response. Dalton Transactions, 2017, 46, 12605-12611.	3.3	17
79	Spatial ions distribution of the bonding interface in <scp>YAG</scp> /Nd:Lu <scp>AG</scp> composite laser ceramic. Journal of the American Ceramic Society, 2017, 100, 5030-5037.	3.8	8
80	Re-clustering of neodymium ions in neodymium, buffer ion-codoped alkaline-earth fluoride transparent ceramics. CrystEngComm, 2017, 19, 4480-4484.	2.6	4
81	Transparent Nd-doped Ca1â^'xYxF2+x ceramics prepared by the ceramization of single crystals. Materials and Design, 2017, 113, 326-330.	7.0	20
82	Ultrafast Saturable Absorption of Core/Shell Colloidal Quantum Dots. Particle and Particle Systems Characterization, 2017, 34, 1600193.	2.3	10
83	Influence of moisture absorption on the synthesis and properties of Y2O3–MgO nanocomposites. Ceramics International, 2017, 43, 40-44.	4.8	25
84	CdTe/CdS Quantum Dots: Effective Saturable Absorber for Visible Lasers. IEEE Journal of Selected Topics in Quantum Electronics, 2017, 23, 1-7.	2.9	19
85	Manipulation and simulations of thermal field profiles in laser heat-mode lithography. Journal of Applied Physics, 2017, 122, .	2.5	7
86	Preparation and Optical Properties of Infrared Transparent 3Y-TZP Ceramics. Materials, 2017, 10, 390.	2.9	11
87	Precipitation and Growth Mechanism of Diverse Sr <sub>5</sub> ( <scp>PO</scp> <sub>4</sub> ) <sub>3</sub> F Particles. Journal of the American Ceramic Society, 2016, 99, 1498-1503.	3.8	13
88	Recrystallization of Er <sup>3+</sup> :CaF <sub>2</sub> in Transparent Fluorophosphate Glassâ€Ceramics with the Coâ€Firing Method. Journal of the American Ceramic Society, 2016, 99, 2971-2976.	3.8	10
89	Geometry Dependent Evolution of the Resonant Mode in ZnO Elongated Hexagonal Microcavity. Scientific Reports, 2016, 6, 19273.	3.3	19
90	Mid-infrared laser emission from Cr:ZnS channel waveguide fabricated by femtosecond laser helical writing. Scientific Reports, 2016, 5, 18365.	3.3	18

#	Article	IF	CITATIONS
91	Origin of arbitrary patterns by direct laser writing in a telluride thin film. RSC Advances, 2016, 6, 45748-45752.	3.6	8
92	Doping limit and site occupation of Yb <sup>3+</sup> in strontium fluoroapatite. RSC Advances, 2016, 6, 88868-88873.	3.6	7
93	Slow and fast absorption saturation of black phosphorus: experiment and modelling. Nanoscale, 2016, 8, 17374-17382.	5.6	46
94	Surfaceâ€Energyâ€Driven Growth of ZnO Hexagonal Microtube Optical Resonators. Advanced Optical Materials, 2016, 4, 126-134.	7.3	19
95	Colloidal quantum-dot-based silica gel glass: two-photon absorption, emission, and quenching mechanism. Nanoscale, 2016, 8, 16440-16448.	5.6	19
96	Two-photon absorption and emission in CsPb(Br/I) <sub>3</sub> cesium lead halide perovskite quantum dots. CrystEngComm, 2016, 18, 7945-7949.	2.6	40
97	Sol–gel derived mesoporous GaAlPO <sub>4</sub> glass for heavy metal ion sequestration. RSC Advances, 2016, 6, 99149-99157.	3.6	8
98	Covalent functionalization of reduced graphene oxide with porphyrin by means of diazonium chemistry for nonlinear optical performance. Scientific Reports, 2016, 6, 23325.	3.3	98
99	Granulation of Y <sub>2</sub> O <sub>3</sub> powders by a vibration method for the preparation of transparent ceramics. RSC Advances, 2016, 6, 105755-105760.	3.6	1
100	Ultrafast Nonlinear Excitation Dynamics of Black Phosphorus Nanosheets from Visible to Mid-Infrared. ACS Nano, 2016, 10, 6923-6932.	14.6	231
101	Optical absorption and mechanism of vacuum-sintered ZrO2-doped Y2O3 ceramics. Journal of the European Ceramic Society, 2016, 36, 4181-4184.	5.7	26
102	Europium doped transparent glass ceramics containing CaF <sub>2</sub> micron-sized crystals: structural and optical characterization. RSC Advances, 2016, 6, 55366-55373.	3.6	15
103	Direct synthesis of large-scale hierarchical MoS <sub>2</sub> films nanostructured with orthogonally oriented vertically and horizontally aligned layers. Nanoscale, 2016, 8, 431-439.	5.6	39
104	Optical identification of layered MoS2via the characteristic matrix method. Nanoscale, 2016, 8, 1210-1215.	5.6	22
105	TiO <sub>2</sub> –multi-walled carbon nanotube nanocomposites: hydrothermal synthesis and temporally-dependent optical properties. RSC Advances, 2016, 6, 20120-20127.	3.6	32
106	Er 3+ -doped oxyfluorogallate glass for 2.7 µm solid-state lasers. Journal of Luminescence, 2016, 172, 331-334.	3.1	18
107	Multi-walled carbon nanotubes covalently functionalized by axially coordinated metal-porphyrins: Facile syntheses and temporally dependent optical performance. Nano Research, 2016, 9, 458-472.	10.4	31
108	Functionalization of reduced graphene oxide with axially-coordinated metal-porphyrins: facile syntheses and temporally-dependent nonlinear optical properties. Inorganic Chemistry Frontiers, 2016, 3, 296-305.	6.0	20

#	Article	IF	CITATIONS
109	Optical Limiting and Theoretical Modelling of Layered Transition Metal Dichalcogenide Nanosheets. Scientific Reports, 2015, 5, 14646.	3.3	236
110	Tunable and white light emitting AlPO4 mesoporous glass by design of inorganic/organic luminescent species. APL Materials, 2015, 3, 046101.	5.1	5
111	Giant twoâ€photon absorption in monolayer MoS <sub>2</sub> . Laser and Photonics Reviews, 2015, 9, 427-434.	8.7	161
112	Preparation of LuAG Powders with Single Phase and Good Dispersion for Transparent Ceramics Using Co-Precipitation Method. Materials, 2015, 8, 5363-5375.	2.9	9
113	Effects of annealing on Cr-sensitized Nd:LuAG laser ceramics. Optical Materials Express, 2015, 5, 2209.	3.0	10
114	Direct Observation of Degenerate Two-Photon Absorption and Its Saturation in WS <sub>2</sub> and MoS <sub>2</sub> Monolayer and Few-Layer Films. ACS Nano, 2015, 9, 7142-7150.	14.6	322
115	Intense multiphoton upconversion of Yb <sup>3+</sup> –Tm <sup>3+</sup> doped β-NaYF <sub>4</sub> individual nanocrystals by saturation excitation. Journal of Materials Chemistry C, 2015, 3, 364-369.	5.5	55
116	Nonlinear optical propagation in a tandem structure comprising nonlinear absorption and scattering materials. Applied Physics Letters, 2014, 104, 021110.	3.3	10
117	Tunable effective nonlinear refractive index of graphene dispersions during the distortion of spatial self-phase modulation. Applied Physics Letters, 2014, 104, .	3.3	84
118	Rapid identification of H5 avian influenza virus in chicken throat swab specimens using microfluidic real-time RT-PCR. Analytical Methods, 2014, 6, 2628.	2.7	12
119	Freeâ€Standing, Singleâ€Crystalline Parallelogram Sb Shallowâ€Doped ZnO Waveâ€Guided Optical Resonators. Advanced Optical Materials, 2014, 2, 1090-1097.	7.3	8
120	Medium-Range Order in Sol–Gel Prepared Al <sub>2</sub> O <sub>3</sub> –SiO <sub>2</sub> Glasses: New Results from Solid-State NMR. Journal of Physical Chemistry C, 2014, 118, 4906-4917.	3.1	61
121	Optical modulation in microsized optical resonators with irregular hexagonal cross-section. Journal of Materials Chemistry C, 2014, 2, 8976-8982.	5.5	11
122	Sol–gel preparation of mesoporous Al2O3–SiO2 glasses: structural evolution monitored by solid state NMR. Journal of Sol-Gel Science and Technology, 2014, 70, 482-490.	2.4	17
123	The effect of La2O3 in Tm3+-doped germanate-tellurite glasses for ~2â€Î¼m emission. Scientific Reports, 2014, 4, 5256.	3.3	43
124	Optical modulation of ZnO microwire optical resonators with a parallelogram cross-section. Nanoscale, 2013, 5, 4123.	5.6	11
125	Tailoring the Luminescence of Europium Ions in Mesoporous AlPO <sub>4</sub> Monolithic Glass. Journal of Physical Chemistry C, 2013, 117, 21916-21922.	3.1	15
126	A novel synthesis and excellent photodegradation of flower-like ZnO hierarchical microspheres. CrystEngComm, 2013, 15, 10272.	2.6	14

#	Article	IF	CITATIONS
127	Single-crystalline tower-like ZnO microrod UV lasers. Journal of Materials Chemistry C, 2013, 1, 202-206.	5.5	55
128	CLASSIFICATION OF SKIN AUTOFLUORESCENCE SPECTRUM USING SUPPORT VECTOR MACHINE IN TYPE 2 DIABETES SCREENING. Journal of Innovative Optical Health Sciences, 2013, 06, 1350036.	1.0	2
129	Thermodynamic-effect-induced growth, optical modulation and UV lasing of hierarchical ZnO Fabry–Pérot resonators. Journal of Materials Chemistry, 2012, 22, 3069.	6.7	11
130	Intense photoluminescence at 27 μm in transparent Er^3+:CaF_2-fluorophosphate glass microcomposite. Optics Letters, 2011, 36, 4347.	3.3	35
131	Homogeneity of Inorganic Glasses: Quantification and Ranking. International Journal of Applied Glass Science, 2011, 2, 137-143.	2.0	5
132	Graphene and Carbon Nanotube Polymer Composites for Laser Protection. Journal of Inorganic and Organometallic Polymers and Materials, 2011, 21, 736-746.	3.7	37
133	Fabrication of large-volume microfluidic chamber embedded in glass using three-dimensional femtosecond laser micromachining. Microfluidics and Nanofluidics, 2011, 11, 111-117.	2.2	26
134	Efficient Energy and Electron Transfer between Donor and Acceptor Chromophores in Aluminophosphate Hybrid Materials. Journal of the Chinese Chemical Society, 2010, 57, 539-546.	1.4	12
135	Large-size oxyfluoride glasses used for vis–IR-transmitting windows. Journal of Non-Crystalline Solids, 2009, 355, 2006-2009.	3.1	13
136	Sol-gel synthesis of sodium-modified AlPO4–SiO2 glasses and structural characterization by solid state NMR. Journal of Materials Chemistry, 2009, 19, 1151.	6.7	15
137	Structural Role of Fluoride in Aluminophosphate Solâ^'Gel Glasses:  High-Resolution Double-Resonance NMR Studies. Journal of Physical Chemistry B, 2007, 111, 10402-10412.	2.6	29
138	Short- and Medium-Range Order in Sodium Aluminophosphate Glasses:Â New Insights from High-Resolution Dipolar Solid-State NMR Spectroscopy. Journal of Physical Chemistry B, 2006, 110, 8946-8958.	2.6	93
139	Performance and structure evolution of fluoindinate glass at high temperatures. Journal of the American Ceramic Society, 0, , .	3.8	2
140	Stable Multiâ€Wavelength Lasing in Single Perovskite Quantum Dot Superlattice. Advanced Optical Materials, 0, , 2200494.	7.3	3